Astronomy & Astrophysics manuscript no. 4u1700+24
January 10, 2014
© ESO 2014

arXiv:1401.2053v1 [astro-ph.HE] 9 Jan 2014

The puzzling symbiotic X-ray system 4U1700+24

A.A. Nucita[1,2], S. Stefanelli[1], F. De Paolis[1,2], N. Masetti[3], G. Ingrosso[1,2], M. Del Santo[4], and L. Manni[1,2]

[1] Department of Mathematics and Physics *"E. De Giorgi"*, University of Salento, Via per Arnesano, CP 193, I-73100, Lecce, Italy
[2] INFN, Sez. di Lecce, via per Arnesano, CP 193, I-73100, Lecce, Italy
[3] INAF – Istituto di Astrofisica Spaziale e Fisica Cosmica di Bologna, via Gobetti 101, I-40129 Bologna, Italy
[4] INAF/IAPS, via del Fosso del Cavaliere, 100, I-00133, Roma, Italy

Submitted: XXX; Accepted: XXX

ABSTRACT

Context. Symbiotic X-ray binaries form a subclass of low-mass X-ray binary systems consisting of a neutron star accreting material from a red giant donor star via stellar wind or Roche lobe overflow. Only a few confirmed members are currently known; 4U 1700+24 is a good candidate as it is a relatively bright X-ray object, possibly associated with the late-type star V934 Her.
Aims. We analysed the archive *XMM*-Newton and Swift/XRT observations of 4U 1700+24 in order to have a uniform high-energy ($0.3-10$ keV) view of the source. Apart from the 2003, 2010, and 2012 data, publicly available but still unpublished, we also took the opportunity to re-analyze a set of *XMM*-Newton data acquired in 2002.
Methods. After reducing the *XMM*-Newton and Swift/XRT data with standard methods, we performed a detailed spectral and timing analysis.
Results. We confirmed the existence of a red-shifted O VIII Ly-α transition (already observed in the 2002 *XMM*-Newton data) in the high-resolution spectra collected via the RGS instruments. The red-shift of the line is found in all the analysed observations and, on average, it was estimated to be $\simeq 0.009$. We also observed a modulation of the centroid energy of the line on short time scales (a few days) and discuss the observations in the framework of different scenarios. If the modulation is due to the gravitational red-shift of the neutron star, it might arise from a sudden re-organization of the emitting X-ray matter on the scale of a few hundreds of km. Alternatively, we are witnessing a uni-polar jet of matter (with typical velocity of $1000-4000$ km s^{-1}) possibly emitted by the neutron star in an almost face-on system. The second possibility seems to be required by the apparent lack of any modulation in the observed X-ray light curve. We also note also that the low-resolution spectra (both *XMM*-Newton and Swift/XRT in the $0.3-10$ keV band) show the existence of a black body radiation emitted by a region (possibly associated with the neutron star polar cap) with typical size from a few tens to hundreds of meters. The size of this spot-like region reduces as the overall luminosity of 4U 1700+24 decreases.

Key words. (X-rays) binaries – (Stars:) binaries: symbiotic – (Stars) neutron – (Stars) individual: 4U 1700+24

1. Introduction

Symbiotic X-ray binaries (SyXBs) form a tiny subclass of Galactic low-mass X-ray binaries (LMXBs) characterized by a red giant star (generally of spectral type M) which loses matter to a compact object, most likely a neutron star (NS), via stellar wind, or (less frequently, as in the case of GX 1+4; Chakrabarty & Roche 1997) Roche lobe overflow. Only seven confirmed members are currently known, while for other candidates like 1RXS J180431.1-273932 (Nucita et al. 2007) follow-up observations allowed us to exclude the SyXB nature (see Masetti et al. 2012 and references therein). However, according to stellar population synthesis studies performed by Lü et al. (2012), between 100 and 1000 of these objects are expected to be in the Galaxy (although one should note that half of the SyXBs considered by the authors were found to be either spurious or unconfirmed cases).

The SyXB subclass only started gaining some attention from the scientific community in the last decade only; however, X-ray studies of these sources are still quite sporadic, with only a handful of objects having been explored in this spectral window (Masetti et al. 2002, 2007a,b, Rea et al. 2005, Paul et al. 2005, Tiengo et al. 2005, Mattana et al. 2006, Patel et al. 2007, Corbet et al. 2008, Marcu et al. 2011, González-Galĺan et al. 2012).

One of these sources is 4U 1700+24. It was discovered (Cooke et al. 1978, Forman et al. 1978) as a relatively bright X-ray object, with variability on both long-term timescales (months to years; Masetti et al. 2002, Corbet et al. 2008) and short-term timescales (tens to thousands of seconds: Garcia et al. 1983, Dal Fiume et al. 1990); This characteristic suggested that the source might be an accreting system; Garcia et al. (1983) proposed the brightlate-type star V934 Her as the optical counterpart of 4U 1700+24 (see also Gaudenzi & Polcaro 1999 and Masetti et al. 2002) on the basis of its position and the detection of emission lines in its ultraviolet spectrum. This association was later confirmed by Masetti et al. (2006) with a *Chandra* X-ray satellite observation that provided a localization of the source with subarcsecond precision.

Send offprint requests to: A.A. Nucita, e-mail: nucita@le.infn.it

Periodicity studies of the object's light curve were performed in X-rays (Masetti et al. 2002, Galloway et al. 2002, Corbet et al. 2008) and optical (Hinkle et al. 2006), without finding any concluding evidence of either orbital or accretor spin modulation.

X-ray spectroscopy of the source, obtained over the last decades (Garcia et al. 1983, Dal Fiume et al. 1990, Masetti et al. 2002), shows a continuum typical of accreting LMXBs, with a thermal component probably originating on or near the accretor and a Comptonized emission detected up to 100 keV. In particular, Masetti et al. (2002) examined the X-ray spectroscopic properties of the source using data collected with several satellites over 13 years, from 1985 to 1998. After this study, Tiengo et al. (2005) published a paper on the X-ray behaviour of 4U 1700+24: the authors analysed an observation collected with the *XMM*-Newton satellite in 2002 and found an emission feature at ≈ 0.5 keV and an emission line at $\simeq 0.64$ keV which was possibly identified as the red-shifted O VIII Ly-α transition.

No further investigations on the X-ray spectroscopic behaviour of 4U 1700+24 have been performed since then; however, three more *XMM*-Newton pointings performed in 2003 and seven Swift/XRT observations made in 2010 and 2012 are publicly available but still unpublished. In this paper we present an analysis of these data, together with an independent examination of the 2002 observation first reported by Tiengo et al. (2005) in order to have a uniform analysis of the whole *XMM*-Newton and Swift/XRT data sets concerning 4U 1700+24. We found that the feature observed at $\simeq 0.5$ keV is possibly an artifact due primarily to the instrumental oxygen edge (see e.g. Armas-Padilla et al. 2013), while we confirm the existence of the $\simeq 0.6$ keV line. Moreover, we found that the line evolves in time.

The present work is structured as follows: Sect. 2 reports the observations and the data analysis; in Sect. 3, the results from these four pointings are presented; whereas Sect. 4 provides a discussion of our results.

2. *XMM*-Newton observation and data reduction

The source 4U1700+24 has been observed several times (see Table 1 for details) by all the X-ray instruments (RGS 1 and 2, EPIC-MOS 1 and 2, EPIC-pn; Jansen et al. 2001, Strüder et al. 2001, and Turner et al. 2001) on board the *XMM*-Newton satellite. Here, we report the observation identification number, the nominal target coordinates (right ascension and declination), the position angle, the observation date together with the start and end time, the nominal duration, and the esposure time after removing the high-energy flares.

The observation raw data files (ODFs) were processed using the *XMM*-Science Analysis System (SAS version 13.0.0) and with the most updated calibration constituent files. To obtain the calibrated low- and high-resolution spectra, we ran the *emchain* and *epchain* tools for the EPIC cameras products, while the *rgsproc* pipeline was executed for the RGS 1 and RGS 2 instruments.

We followed the standard analysis recipes described in the XRPS User's manual (2008). In particular, we extracted the light curves above 10 keV for the full MOS and pn cameras. We then identified and discarded parts of the observations affected by high levels of background activity, by using a threshold of 0.35 and 0.40 counts s^{-1} for the two MOS and pn, respectively. For each observation, the exposure time resulting from this procedure is reported (in ks) in the last column of Table 1 for the MOS 1, 2 and pn, respectively. The events collected during the good time intervals were only used in the spectral analysis, being the timing analysis performed without applying any time filters to avoid the introduction of artifacts.

The X-ray emission from the source was first extracted from a circular region centred on the nominal position of 4U 1700+24 as determined by Masetti et al. (2002) when analyzing the *Chandra*/HRC data ($\alpha = 17^{\rm h}\ 06^{\rm m}\ 34.517^{\rm s}$, $\delta = +23^0\ 58'\ 18.66''$, with errors on both coordinates of $\simeq 0.6''$) and with a radius chosen to contain at least 80% of the total source energy. The background signal was accumulated from circular regions on the same chip.

We noted that the observations labeled as 0155960601, 0151240301, and 0151240201 were affected by pile-up. This effect consists in two or more photons hitting nearby CCD pixels during an exposure, thus producing an event which mimics a single, larger energy photon. If not severe, the pile-up effect can be mitigated by following the method described in the XRPS User's manual (2008). In particular, we extracted the source signal by using an annular region centred on the source nominal coordinates with inner and outer radii of $\simeq 10''$ and $\simeq 40''$, respectively. With this choice, and in accordance with the signal found by Tiengo et al. (2005) when analyzing the 2002 observation, we were able to correct the pile-up for the EPIC pn data, but not for the MOS 1 and 2 cameras for which the correction would have greatly reduced the number of good counts. Consequently, we avoided using these data to prevent spurious effects in the spectral and timing analysis.

Finally, source and background X-ray spectra, together with the associated ancillary and response matrix files, were extracted and imported within XSPEC (Arnaud et al. 2007) for a simultaneous fitting procedure.

3. Swift/XRT observation and data reduction

Swift/XRT observed 4U 1700+24 in 2010 with two dedicated pointings and in 2012 with five observations, because the source was in the same field of view as the gamma ray burst GRB121202 A (see Table 2 for details on the archive data sets).

The Swift data were analysed using standard procedures (Burrows et al., 2005) and the latest calibration files available at http : //heasarc.nasa.gov/docs7swift/analysis/. In particular, we processed the XRT products with the *xrtpipeline* (v.0.12.6) tasks, applied standard screening criteria by using ftools (Heasoft v.6.13.0), and extracted with *xselect* the source spectra and light curves (in the 0.3-10 keV band) from a circular region (with radius of $\simeq 40''$) centred on the nominal coordinates of the target. When possible, the background spectra and light curves were also extracted from circular regions. We noted that the 2012 Swift/XRT observations were affected by pile-up because the corresponding source count rates were above $\simeq 0.5$ count s^{-1}. Thus, we followed the recipe presented in the Swift on-line threads[1] and discarded the central part (up to $\simeq 15''$) of the source extraction region until the source count rate was below the threshold value. We then used the *xrtmkarf* task to create the ancillary response files and

[1] See http : //www.swift.ac.uk/analysis/xrt/pileup.php

Table 1. Log of the archive *XMM*-Newton observations analysed in this paper.

OBS. ID	REV	NOM. RA (deg)	NOM. DEC (deg)	POS. ANGLE (deg)	DATE (yr-m-d)	START (h:m:s)	END (h:m:s)	NOM.DUR. (ks)	EXP. TIME (ks)
0155960601 *	489	256.64370	23.97183	295.63034	2002-08-11	15:55:49.0	19:32:02.0	13	−, −, 3.2
0151240301 *	593	256.64385	23.97183	79.403876	2003-03-07	01:08:08.0	04:32:20.0	12	−, −, 1.3
0151240201 *	594	256.64385	23.97183	79.399512	2003-03-09	01:03:49.0	04:27:57.0	12	−, −, 5.5
0151240401	673	256.64385	23.97183	294.30723	2003-08-13	15:23:12.0	19:40:38.0	15	9.4, 9.2, 7.8

Note: The observations labelled with an asterisk presented pile-up in the EPIC cameras. We were able to correct for the pile-up only the EPIC pn data. Hence, in these cases, we avoided using the MOS 1 and MOS 2 events in order to prevent spurious effects (see text for details); as a consequence, a symbol − appears in the last column.

Table 2. Log of the archive Swift/XRT observations analysed in this paper.

OBS. ID	DATE (yr-m-d)	START (h:m:s)	END (h:m:s)	EXP. TIME (ks)
0009080001	2010-05-30	20:29:06	23:39:56	1.4
0009080002	2010-06-04	12:55:00	00:16:58	9.7
0054025500 *	2012-12-02	05:07:33	13:12:24	12.8
0054025501 *	2012-12-02	13:13:56	23:14:27	6.4
0054025502 *	2012-12-03	14:56:26	23:03:44	5.3
0054025503 *	2012-12-04	00:47:17	10:28:36	5.8
0054025504 *	2012-12-05	13:21:41	18:11:36	5.9

Note: The observations labeled with an asterisk presented pile-up.

took into account the corrections for the different extraction areas of the source and background and for vignetting. Finally, the light curves were background corrected.

4. Results

4.1. XMM-Newton RGS spectral analysis of 4U1700+24

Our study of the *X*-ray properties of 4U1700+24 started with the analysis of the first order-spectra obtained by the *XMM*-Newton gratings. The spectral resolution of RGS in the first-order spectrum is FWHM=72 mÅ and the calibration in wavelength is accurate up to 8 mÅ , corresponding to FWHM$\simeq$ 620 km s^{-1} and $\Delta v \simeq 69$ km s^{-1} at 35 Å (*XMM*-Newton Users Handbook 2009). In the following, we use the unbinned RGS 1 and RGS 2 spectra for the quantitative analysis and searched for emission lines.

We then imported the spectra (and the associated response matrices) within XSPEC and simultaneously fit the data. In this respect, the phenomenological spectral analysis followed a local fit method[2], i.e. the unbinned spectra were first divided in intervals of $\simeq$ 100 channels wide and then Gaussian profiles were added to account for all identified emission lines. In this procedure, the line energy, as well as its width and normalization were considered as free parameters of the fit. In addition, the local continuum was modelled as a power law with a fixed photon index $\Gamma = 1$ and free normalization. In the fit procedure, consistently with Tiengo et al. (2005), we fixed the column density of Galactic neutral hydrogen to the average value[3] observed along the line of sight towards 4U1700+24, i.e. 4.4×10^{20} cm^{-2} (Dickey & Lockman 1990). For line doublets and triplets and for emission lines close to free-bound transitions, the relative distance among the central energies was frozen to the value predicted by the atomic physics.

We used the C-statistics (Cash 1979) as the estimator of the goodness of the performed fit and, for any line initially recognized as such by eye, the feature was considered *detected* if, repeating the fit without any Gaussian profile, the newly obtained value of the statistics differed by at least 2.3 from the previous one. This choice corresponds to 68% confidence level (or, equivalently, 1 σ for one interesting parameter) for the detected emission line (Arnaud et al., 2007). Finally, our estimate of the error associated with the centroid energy was evaluated as the quadratic sum of the error in output from XSPEC and the calibration uncertainty quoted above.

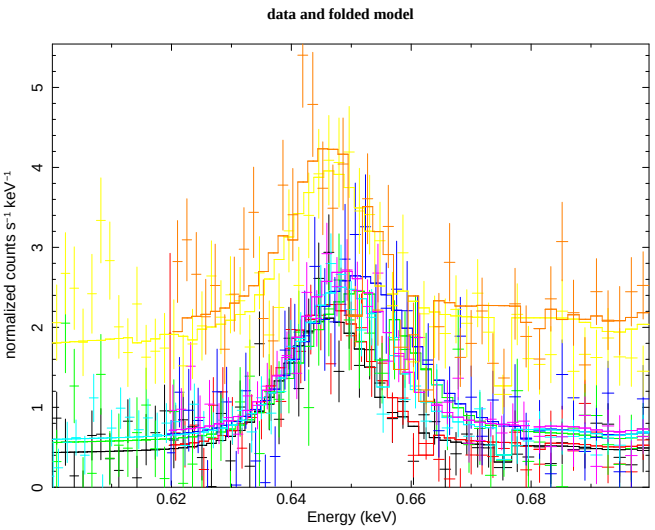

Fig. 1. A zoom of the RGS 1 and 2 spectra of 4U1700+24 around the O VIII Ly-α emission line (at about $\simeq$ 19 Å) for all the observations quoted in Table 1. The spectra were binned in order to have a signal-to-noise ratio of 5 in each bin, and we give the horizontal axis in energy instead of wavelength. The data in yellow/orange (corresponding to the 2002 observation, i.e. 0155960601) clearly show a large continuum component with respect to the other data sets, thus reflecting the high activity of the source at that time. The solid lines represent the best-fit model as described in the text.

In particular, this procedure resulted in the identification of an emission feature at $\simeq$ 0.645 keV ($\simeq$ 19 Å), i.e. consistent with that already observed by Tiengo et al. (2005) in the RGS 1 and 2 spectra of the 2002 observation. We do still identify the same line in all the subsequent *XMM*-Newton observations considered in this work. In Fig. 1, we give a zoom of the RGS 1 and 2 spectra around the identified emission line (binned in order to have 5σ per bin,

[2] Although in a different context, the *local fit method* is described in Guainazzi & Bianchi (2007).

[3] We used the on-line N_H calculator (available at http://heasarc.nasa.gov/cgi-bin/Tools/w3nh/w3nh.pl) to get the average column density.

and with the horizontal axis in energy) of 4U1700+24, for all the observations quoted in Table 1. We note that the data in yellow/orange correspond to the 2002 observation (Obs. ID 0155960601) and clearly show a continuum component larger than that present in the other data sets; this reflects the high activity of the source at that time (see also next paragraph).

Some emission lines within a few σ of the observed feature are found in the CHIANTI database (Dere et al., 2001), with the Ly-ϵ line of the *NVII* having a centroid energy position compatible with that observed in our spectra. However, as first discussed by Tiengo et al. (2005), the probability of the occurrence of this transition is very low, thus pushing toward the interpretation of this line as the red-shifted Ly-α transition of the H-like oxygen, i.e. the OVIII feature with a rest-frame wavelength of 18.9671Å .

In Table 3, we give the best-fit parameters (C_{Stat} = 2234.33 for 2044 degrees of freedom) obtained via the method described above[4] for the emission line observed at $\simeq 19$ Å for each of the *XMM*-Newton observations analysed in this work. Here, we report the mean time of the observation (in Modified Julian Date, MJD), the line normalization, the best-fit central energy (E_{obs}) and the line width (σ_{obs}). Assuming that the observed emission line is the red-shifted Ly-α transition of the H-like oxygen (OVIII), in the last two columns we give the red-shift factor and associated equivalent velocity (defined as $\Delta\lambda/\lambda = v/c$, being c the speed of light), respectively.

On average, the emission line has an energy of $\simeq 0.648$ keV, corresponding to a wavelength of $\simeq 19.136$Å , and an average red-shift of $\simeq 0.009$ (see also below). In Figure 2, we show the position (upper panel) in keV, the line width (middle panel), and the red-shift factor (bottom panel) of the O VIII Ly-α line as a function of the observation time (here defined as the average time of each exposure) in MJD. We note that the line energy for observation 0155960601 is consistent with that already derived by Tiengo et al. (2005). We first fitted the central energy of the emission feature, its width, and the red-shift factor (assuming the rest-frame energy to be that of the O VIII Ly-α line) with constant values (see the dot-dashed lines in the three panels in Fig. 2) finding 0.648 ± 0.001 keV ($\chi^2 = 2.8$ for 3 dof), 0.0067 ± 0.001 keV ($\chi^2 = 0.45$ for 3 dof), and 0.009 ± 0.001 ($\chi^2 = 2.1$ for 3 dof), respectively. Then, we searched for a global trend in the data by using a linear model as a fitting function. Assuming that the overall behaviour of the data varies linearly with time, we obtained the rate of changes of the interested parameters to be $(5.9 \pm 5.4) \times 10^{-6}$ keV day^{-1} ($\chi^2 = 3.6$ for 2 dof), $(2.8 \pm 5.4) \times 10^{-6}$ keV day^{-1} ($\chi^2 = 0.5$ for 2 dof), and $(-1.1 \pm 0.8) \times 10^{-5}$ day^{-1} ($\chi^2 = 2.1$ for 2 dof), respectively. Although a close inspection of Fig. 2 might allow us to conclude that the emission line position changes on time scales of $\simeq 2$ days (see e.g. the bottom panel where this effect is amplified by the fact that the red-shift factor is given and also the log of the observations in Table 1), a constant model seems to be preferred when one considers the long-term trend.

We also tried the identification of the most intense lines of He-like ions of oxygen in the range 5-35 Å, i.e. the transitions between the $n = 2$ shell and the $n = 1$ ground

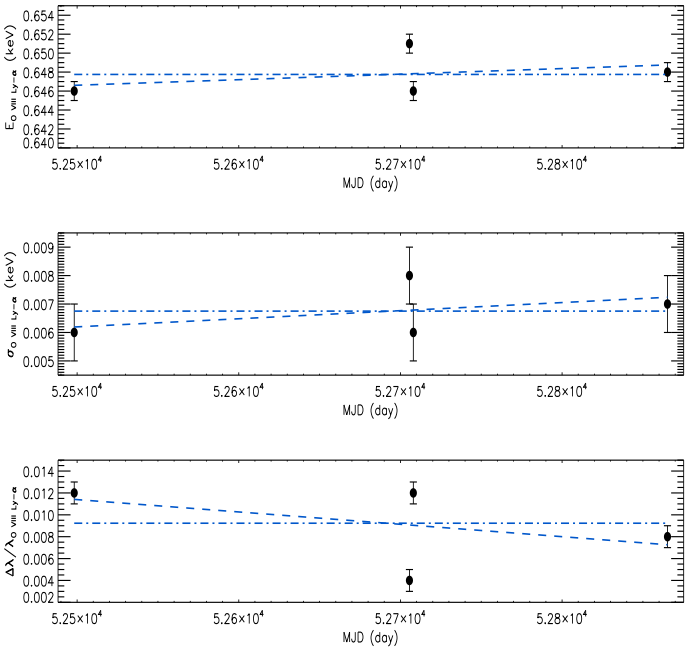

Fig. 2. Here, we show the centroid position in keV (upper panel) as determined by the Gaussian line fit, the line width (middle panel), and the red-shift factor of the O VIII Ly-α line identified in the high-resolution spectra of 4U1700+24 as a function of the observation time (defined as the average time of each exposure) in modified Julian date. In each panel, the dot-dashed line represents a fit with a constant, while the dashed line accounts for any linear trend possibly associated with the data (see text for details).

state shell as the resonance line, **r** : $1s^2\ ^1S_0$-$1s2p\ ^1P_1$, the two inter-combination lines (often blended), **i** : $1s^{21}S_0$-$1s2p\ ^3P_{2,1}$, and the forbidden feature, **f** : $1s^{21}S_0$-$1s2s^3S_1$. These transitions are particularly important since, as demonstrated by Porquet & Dubau (2000), their relative emission strengths are good indicators of the physical conditions of the gas density and temperature.

Because of the poor statistics of the RGS data, the fit the O VII complex with a model constituted by a power law and three Gaussians (with all the parameters free, except the relative distances among the lines, as well as the continuum power law index) did not converge. We then used a different approach and, in particular, we fixed the centroid energy of the interested lines to that expected by the atomic physics, after correcting for the average red-shift ($\Delta\lambda/\lambda \simeq 0.009$) previously found. We also set all the line widths to zero. Leaving as free parameters the Gaussian line and power law normalizations allowed us to get a reasonable fit (see Fig. 3) characterized[5] by $C_{Stat} = 664.3$ for 520 degrees of freedom. However, this procedure only resulted in upper limits to all the line normalizations, thus making impossible to infer the physical condition of the X-ray emitting gas. In this case, our best-fit model works only as a guide for the eye when searching for the O VII complex lines. In this respect, we note that the RGS data show the existence (although with a signal-to-noise ratio

[4] When repeating the fit without the Gaussian line profile, the new value of the statistics is $C_{Stat} = 3270.75$ for 2056 degrees of freedom, thus implying the necessity of a Gaussian component.

[5] Performing the fit procedure with a normalized power law only resulted in a best-fit with $C_{Stat} = 673.0$ for 532 degrees of freedom. In the framework of the local method discussed in the text, the comparison of this best-fit with the previous one allows us to be confident with the existence of the O VII complex.

Table 3. For each of the *XMM*-Newton observations, we give the main best-fit parameters (normalization, centroid position energy E_{obs}, line width σ_{obs}, and wavelength λ_{obs}) of the emission feature observed at $\simeq 19$ Å (see text for details).

OBS. ID	MJD (day)	N_2 ($cm^{-2}s^{-1}$)	E_{obs} (keV)	σ_{obs} (keV)	λ_{obs} (Å)	$\Delta\lambda/\lambda$	v km s^{-1}
0155960601	52498.21	$(9.0 \pm 1.0) \times 10^{-4}$	$0.646^{+0.001}_{-0.001}$	$0.006^{+0.001}_{-0.001}$	$19.195^{+0.030}_{-0.030}$	$0.012^{+0.001}_{-0.002}$	3600^{+300}_{-600}
0151240301	52705.58	$(1.1 \pm 0.2) \times 10^{-3}$	$0.651^{+0.001}_{-0.001}$	$0.008^{+0.001}_{-0.001}$	$19.048^{+0.030}_{-0.030}$	$0.004^{+0.002}_{-0.002}$	1200^{+600}_{-600}
0151240201	52707.99	$(8.4 \pm 1.0) \times 10^{-4}$	$0.646^{+0.001}_{-0.001}$	$0.006^{+0.001}_{-0.001}$	$19.195^{+0.030}_{-0.030}$	$0.012^{+0.002}_{-0.002}$	3600^{+600}_{-600}
0151240401	52865.22	$(9.9 \pm 1.0) \times 10^{-4}$	$0.648^{+0.001}_{-0.001}$	$0.007^{+0.001}_{-0.001}$	$19.136^{+0.030}_{-0.030}$	$0.009^{+0.001}_{-0.002}$	2400^{+300}_{-600}

less than $\simeq 1$) of emission lines in the positions where the O VII complex lines are expected; this makes us confident that the line identified at $\simeq 0.19$ Å is really the O VIII Ly-α transition red-shifted by an average red-shift of $\simeq 0.009$.

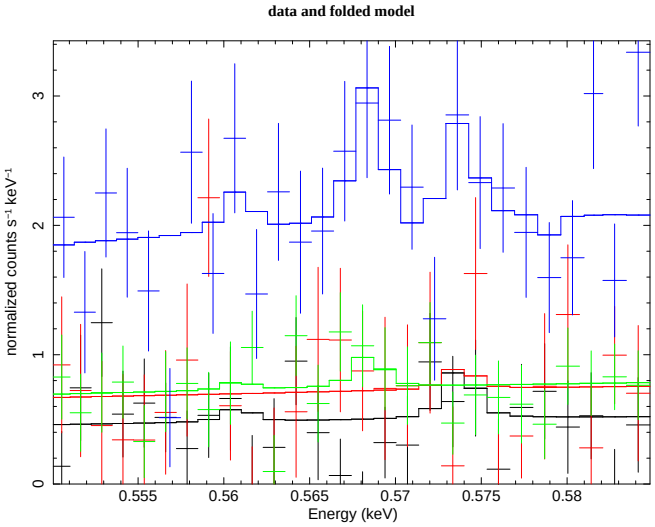

Fig. 3. A zoom around the O VII triplet (data points rebinned in order to have a signal-to-noise ratio of 5 in each bin) and the best-fit model superimposed after red-shifting the rest-frame energy of the complex by $\Delta\lambda/\lambda \simeq 0.009$, i.e. the energy found when analyzing the O VIII Ly-α.

4.2. XMM-Newton EPIC spectral analysis of 4U1700+24

Following Masetti et al. (2002) and Tiengo et al. (2005), we simultaneously fitted all the low-resolution spectra of 4U1700+24 with an absorbed black body plus Comptonization (COMPST in XSPEC). As in the case of the RGS analysis, we fixed the Galactic neutral hydrogen column density to the average value observed towards the target, i.e. 4.4×10^{20} cm^{-2} (Dickey & Lockman 1990). However, we noted the existence of large residuals at low energies (close to $\simeq 0.5$ keV and $\simeq 0.6$ keV) particularly similar to the typical shape of emission lines. The existence of a broad emission ($\sigma \simeq 0.1$ keV) line at $\simeq 0.5$ keV was already noted by Tiengo et al. (2005) and explained as due to the blending of several lines possibly observed in the RGS data, but no other emission line feature was reported. We note that the feature observed at $\simeq 0.5$ keV may be due to the instrumental absorption oxygen edge at 23 Å as recently found by Armas-Padilla et al. (2013). For simplicity, we model this feature as a large Gaussian line after verifying that the use of the model EDGE in XSPEC to account for its shape did not dramatically improve our best-fit.

The existence of something missing in the model at $\simeq 0.6$ keV is particularly clear in the residuals associated to the 2003 EPIC spectra; we interpret this feature as the fingerprint of the O VIII Ly-α observed in the RGS data. Thus, our best-fit model consisted of an absorbed black body plus a Comptonization to which two emission lines (the instrumental feature at $\simeq 0.5$ keV and a real emission line at $\simeq 0.6$ keV) were added. For convergence purposes, we left the centroid energy (and the associated width) of the broad feature observed at $\simeq 0.5$ keV as free parameters, but fixed the position and width of the O VIII Ly-α line to the value obtained when analyzing RGS 1 and 2 spectra (see Table 3). With reference to Fig. 4 (left panel), the black, green, blue, and red data points correspond to the EPIC pn data of the observations 0155960601, 0151240301, 0151240201, and 0151240401, respectively. The pile-up affected most of the data sets, so that the MOS 1 and MOS 2 data (purple and cyan points in the same figure) were only available for the last observation. The EPIC best-fit parameters ($\chi^2 = 1.3$ for 1379 degree of freedom - d.o.f) are reported in the first four rows of Table 4. Here, kT_{BB} is the temperature of the black-body component, kT_c and τ the temperature and optical depth of the Comptonization, E_1 and σ_1 the broad feature (at $\simeq 0.5$ keV) position and line width, respectively. All the normalizations of the model components are free to vary. In particular, N_{BB}, N_C, N_1 and N_2 are the black body, the Comptonization, the broad feature and the O VIII Ly-α line normalizations, respectively. In the BBODYRAD normalization, $R_{\rm km}$ and D_{10} are the source radius (in units of km) and distance (in units of 10 kpc), respectively. For the COMPST normalization, N represents the total number of photons from the source and f a factor depending on the injected photon energy and spectral index.

In Table 5, we also give the flux in the same band for each of the *XMM*-Newton observations (first four rows) and the estimated fluxes in the energy bands $0.3-2$ keV, $2-10$ keV, and $0.3-10$ keV , respectively. We note that the absorbed 0.3-10 keV band flux results in 2.35×10^{-10} erg cm $^{-2}$ s $^{-1}$ when averaged over the four *XMM*-Newton observations. As can be seen in the table, the source was in high state during the 2002 observation (see also Tiengo et al. 2005), because the flux was a factor of 2 larger than the average value. We also note that archival EXOSAT, ROSAT, ASCA, RXTE, and BeppoSAX observations (spanning the years 1985-1998) have shown that the X-ray emission from the source appears to become harder as its luminosity increases (see e.g. Table 2 in Masetti et al. 2002). However, we did not find this behaviour in the *XMM*-Newton data analysed in the present paper. We also note that, based on

Table 4. The best fit model describing the EPIC data (first four rows) and Swift/XRT data (last seven rows) consists in an absorbed black body plus a Comptonization to which two emission lines (at $\simeq 0.5$ keV and $\simeq 0.6$ keV) were added (see text for details).

ObsID	kT_{BB} (keV)	N_{BB} R^2_{km}/D^2_{10}	kT_c (keV)	τ	N_C $Nf/4\pi D^2$	E_1 (keV)	σ_1 (keV)	N_1 ($cm^{-2}s^{-1}$)	N_2 ($cm^{-2}s^{-1}$)
0155960601	$0.90^{+0.09}_{-0.06}$	$9.00^{+1.16}_{-2.33}$	$2.11^{+0.08}_{-0.06}$	$34.56^{+0.93}_{-2.20}$	$0.0183^{+0.0007}_{-0.0004}$	$0.464^{+0.028}_{-0.011}$	$0.131^{+0.009}_{-0.024}$	$0.017^{+0.001}_{-0.003}$	≤ 0.0004
0151240301	$0.82^{+0.07}_{-0.03}$	$6.94^{+1.76}_{-1.39}$	$2.12^{+0.20}_{-0.09}$	$27.93^{+2.68}_{-2.68}$	$0.0072^{+0.0005}_{-0.0006}$	$0.485^{+0.020}_{-0.028}$	$0.093^{+0.035}_{-0.024}$	$0.005^{+0.002}_{-0.001}$	$0.0007^{+0.0005}_{-0.0004}$
0151240201	$1.13^{+0.10}_{-0.10}$	$2.66^{+0.24}_{-0.26}$	$2.45^{+0.45}_{-0.22}$	$24.00^{+1.88}_{-3.60}$	$0.0071^{+0.0003}_{-0.0002}$	$0.490^{+0.012}_{-0.011}$	$0.043^{+0.014}_{-0.012}$	$0.0019^{+0.0004}_{-0.0004}$	$0.0010^{+0.0001}_{-0.0001}$
0151240401	$0.71^{+0.05}_{-0.05}$	$6.98^{+2.25}_{-1.41}$	$1.96^{+0.05}_{-0.05}$	$33.07^{+1.88}_{-1.27}$	$0.0075^{+0.0002}_{-0.0004}$	$0.487^{+0.008}_{-0.022}$	$0.108^{+0.018}_{-0.010}$	$0.007^{+0.001}_{-0.001}$	$0.0007^{+0.0001}_{-0.0003}$
0009080001	$1.02^{+0.11}_{-0.08}$	$0.50^{+0.10}_{-0.10}$	(2.16)	$16.29^{+3.44}_{-2.89}$	$0.0008^{+0.0001}_{-0.0001}$	–	–	–	$0.0003^{+0.0001}_{-0.0001}$
0009080002									
0054025500	$0.89^{+0.19}_{-0.13}$	$5.02^{+3.20}_{-1.96}$	(2.16)	$28.96^{+2.88}_{-3.10}$	$0.0070^{+0.0008}_{-0.0009}$	–	–	–	$0.0012^{+0.0005}_{-0.0005}$
0054025501	$1.05^{+0.28}_{-0.23}$	$2.3^{+2.0}_{-1.0}$	(2.16)	$27.34^{+5.34}_{-9.70}$	$0.0040^{+0.0008}_{-0.0005}$	–	–	–	$0.0009^{+0.0005}_{-0.0001}$
0054025502	$0.77^{+0.17}_{-0.10}$	$5.6^{+4.1}_{-2.6}$	(2.16)	$32.58^{+7.90}_{-4.90}$	$0.0031^{+0.0008}_{-0.0005}$	–	–	–	$0.0011^{+0.0005}_{-0.0005}$
0054025503	$0.98^{+0.30}_{-0.16}$	$4.7^{+3.5}_{-1.9}$	(2.16)	$31.94^{+9.30}_{-3.90}$	$0.004^{+0.001}_{-0.001}$	–	–	–	$0.0013^{+0.0006}_{-0.0006}$
0054025504	$0.88^{+0.29}_{-0.17}$	$1.4^{+1.4}_{-0.7}$	(2.16)	$28.90^{+4.28}_{-4.80}$	$0.0020^{+0.0003}_{-0.0003}$	–	–	–	$0.0011^{+0.0003}_{-0.0003}$

a set of *Chandra*/HRC observations, the source again appeared in a high state in April 2005 (with a 2-10 keV flux of $\simeq 2 \times 10^{-10}$ erg cm $^{-2}$ s $^{-1}$ corresponding to a luminosity of $\simeq 4 \times 10^{33}$ erg cm s $^{-1}$, Masetti et al. 2006).

We also note that the black-body component required by the best-fit model allowed us to estimate the radius of the X-ray emitting region to be $\simeq 30-130$ m, i.e. consistent with the expected size of a polar cap emission in a NS.

4.3. Swift/XRT spectral analysis results

The 2010 and 2012 Swift/XRT source spectra (as well as the corresponding background, ancillary, and response matrix files) were imported within XSPEC, grouping together the spectra acquired in 2010. We note that when a row is empty, each parameter remains unchanged with respect to the previous value. Each spectrum was rebinned with a minimum of 25 counts per energy bin. We first tried to use the model providing the best-fit for the *XMM*-Newton EPIC data (see the previous section), but soon we realized that the Gaussian line component at $\simeq 0.5$ keV is not required. On the contrary, residuals appeared at $\simeq 0.6$ keV, thus forcing us to maintain a Gaussian component to account for this line feature: in particular, we fixed (as before) the line centroid energy to the average value $\simeq 0.646$ keV. In order to avoid bad convergences, we fixed the the temperature parameter kT_c of the COMPST component to the average value ($\simeq 2.16$ keV) estimated with the *XMM*-Newton EPIC data only, while leaving the optical depth τ and the normalizations of the model components free to vary.

The best-fit procedure ($\chi^2 = 1.2$ for 621 d.o.f.) resulted in the parameter values reported in the last seven rows of Table 4 (from which one can note that the spectral properties of 4U1700+24 did not change substantially) and in the estimates of the 0.3-2.0 keV, 2.0-10.0 keV, and 0.3-10.0 keV band fluxes (see Table 5), respectively. The best-fit model is superimposed on the Swift/XRT data in the right panel in Fig. 4. As one can note, in accordance with the *XMM*-Newton data, a decrease in the X-ray luminosity is always accompanied by a decrease in the emitting region size. In particular, the 2010 observations clearly show that the black-body component may come from an area with a radius that is at least one fourth of that estimated with the 2003 *XMM*-Newton data.

4.4. XMM-Newton and Swift/XRT temporal analysis results

As discussed before, when extracting the light curve of the target, we did not filter out any period of large background activity as this procedure might introduce spurious features in the timing analysis. Hence, we used the original event list (corrected for the solar system barycenter when needed) files and extracted the light curves in the $0.3 - 10$ keV energy band (and bin size of 10 seconds) for the source and background. In this procedure, we avoided using the data affected by severe pile-up while, for the observation 0151240401, all the EPIC cameras were used to get a final (averaged) light curve. The obtained (synchronized) light curves were given in input to the SAS task *epiclccorr* to account for the background subtraction and for the absolute and relative corrections. The EPIC light curves associated with the four observations analysed in this work (see Table 1) are shown in the four first panels of Fig. 5. During the four *XMM*-Newton observations, the target had an average count rate of 105 ± 7 count s^{-1}, 35 ± 4 count s^{-1}, 28 ± 3 count s^{-1}, and 18 ± 2 count s^{-1}, respectively: clearly, as also discussed before, the target was characterized by a high state during the 2002 observation.

For 2010 and 2012 Swift/XRT observations, we extracted the source and background light curves (in the 0.3-10 keV energy band and bin-size of 10 sec) by using the *xselect*, accounting for the pile up when necessary. Since these light curves were also synchronized, we subtracted the background and scaled for the extraction areas by using the *lcmath* tool. The Swift/XRT light curves are reported in the last two panels of Fig. 5 with, in particular, the 2010 time series on the left and the 2012 on the right part of the figure, respectively. We note that 4U 1700+24 had an average count rate of 0.27 ± 0.23 count s^{-1} in 2010, and 0.47 ± 0.43 count s^{-1} in 2012.

The source is clearly variable and we gave an estimate of this temporal variability by using the normalized excess variance (σ^2_{NXS}; see e.g. Nandra et al. 1997 and Edelson et al. 2002) to which we associated an uncertainty according to eq. (11) in Vaughan et al. (2003). In each panel in Fig. 5, we give the excess variance for the EPIC 0.3-10 keV light

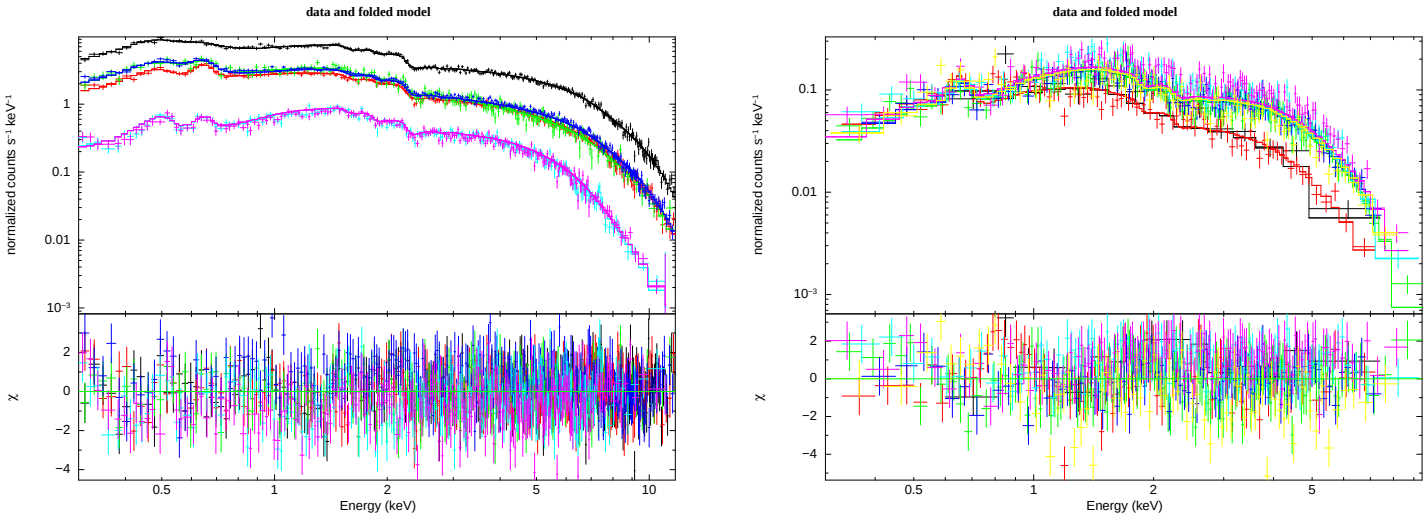

Fig. 4. Left panel: the EPIC spectra of 4U1700+24 during the four observations analysed in this work. Black, green, blue, and red data points correspond to the EPIC pn data of the observations 0155960601, 0151240301, 0151240201, and 0151240401, respectively. Since the pile-up affected most of the data sets, MOS 1 and MOS 2 data (purple and cyan data points) were only available for the last observation (i.e. 0151240401). Here, the solid lines correspond to the best-fit model described in the text. Right panel: the Swift/XRT spectra of 4U1700+24 during the 2010 and 2012 observations (data points) together with the best-fit model (solid lines). Here, the black and red data correspond to the Swift observations 0009080001 and 0009080002, respectively while the other data sets shown (purple, blue, yellow, green and cyan) correspond to the observation IDs from 0054025500 to 0054025504 of Table 4.

Table 5. The $0.3-2$ keV, $2-10$ keV and $0.3-10$ keV band fluxes together with the estimated luminosity (full band) for a source distance of $\simeq 420$ pc.

ObsID	MJD (day)	$F_{0.3-2.0\rm kev}$ (10^{-10} erg cm $^{-2}$ s $^{-1}$)	$F_{2-10.0\rm kev}$ (10^{-10} erg cm $^{-2}$ s $^{-1}$)	$F_{0.3-10.0\rm kev}$ (10^{-10} erg cm $^{-2}$ s $^{-1}$)	$L_{0.3-10.0\rm kev}$ (10^{34} erg s $^{-1}$)
0155960601	52498.22	$0.669^{+0.006}_{-0.021}$	$4.35^{+0.02}_{-0.12}$	$5.02^{+0.03}_{-0.17}$	$1.060^{+0.010}_{-0.040}$
0151240301	52705.58	$0.290^{+0.005}_{-0.021}$	$1.23^{+0.02}_{-0.19}$	$1.52^{+0.03}_{-0.16}$	$0.320^{+0.010}_{-0.040}$
0151240201	52707.99	$0.245^{+0.005}_{-0.004}$	$1.25^{+0.01}_{-0.09}$	$1.49^{+0.01}_{-0.08}$	$0.310^{+0.002}_{-0.020}$
0151240401	52865.22	$0.284^{+0.002}_{-0.004}$	$1.41^{+0.01}_{-0.03}$	$1.69^{+0.01}_{-0.04}$	$0.355^{+0.002}_{-0.010}$
0009080001	55346.92	$0.031^{+0.014}_{-0.008}$	$0.080^{+0.015}_{-0.007}$	$0.110^{+0.020}_{-0.010}$	$0.023^{+0.013}_{-0.006}$
0009080002	55351.78				
0054025500	56263.38	$0.246^{+0.007}_{-0.020}$	$1.30^{+0.06}_{-0.10}$	$1.54^{+0.06}_{-0.13}$	$0.324^{+0.013}_{-0.027}$
0054025501	56263.76	$0.145^{+0.006}_{-0.016}$	$0.773^{+0.093}_{-0.146}$	$0.920^{+0.180}_{-0.160}$	$0.193^{+0.038}_{-0.034}$
0054025502	56264.79	$0.143^{+0.005}_{-0.016}$	$0.739^{+0.045}_{-0.142}$	$0.880^{+0.110}_{-0.160}$	$0.185^{+0.023}_{-0.034}$
0054025503	56265.23	$0.186^{+0.007}_{-0.037}$	$1.09^{+0.08}_{-0.22}$	$1.27^{+0.10}_{-0.27}$	$0.267^{+0.021}_{-0.057}$
0054025504	56266.66	$0.077^{+0.003}_{-0.012}$	$0.373^{+0.029}_{-0.086}$	$0.450^{+0.030}_{-0.093}$	$0.095^{+0.006}_{-0.020}$

curve with a bin-size of 10 seconds. Keeping in mind that negative values of σ^2_{NXS} indicate the absence of or very small variability in the time series, we conclude that the 4U1700+24 light curve shows a certain degree of intrinsic variability which seems to be constant in time. Consistently with the results of Masetti et al. (2002), a variability on time-scales of tens to thousands of seconds can be identified in the high-energy light curve.

We searched for periodic modulations in the time range from 20 s to a few hours by using the the Lomb-Scargle technique (Scargle 1982). We tested the significance of each peak observed in the periodogram by simulating 5000 simulated red-noise light curves each of which with the same statistical properties (mean, variance, time gaps, and red-noise index) as the observed time series following the method described in Timmer & Koenig (1995). For each simulated light curve, we evaluated the Lomb-Scargle periodogram and calculated the *global* probability as explained in Benlloch et al. (2001). In particular, the global significance of a peak at a given frequency and with given amplitude is evaluated by counting the number of peaks with the same height (or larger) in the full range of tested frequencies. As a result, we did not detect any clear periodicity with significance larger than $\simeq 1\sigma$.

5. Discussion and conclusions

The large collecting area of the *XMM*-Newton telescope allowed us to study in detail the accreting binary 4U 1700+24. By using the high spectral resolution of the RGS instruments, we identified an emission line at $\simeq 0.6$ keV (first observed by Tiengo et al. 2005 in 2002), also present in the pn spectrum of the source. We associated the observed emission feature with the O VIII Ly-α transition red-shifted

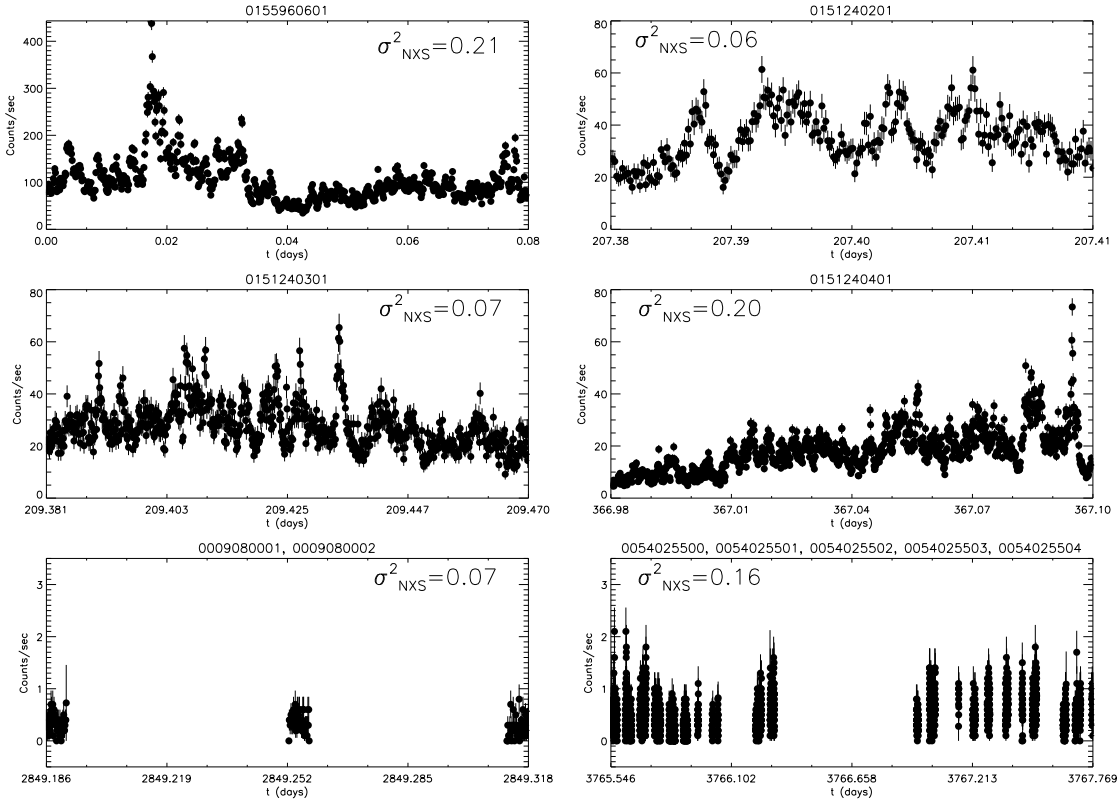

Fig. 5. The *XMM*-Newton and Swift/XRT light curves associated to all the observations analysed in this work (see Table 1) are shown in separated panels. In each panel, we also give the estimate of the excess variance of the *X*-ray signal during each observation. Time is in days from the beginning of the 2002 *XMM*-Newton observation.

by the quantity $\Delta\lambda/\lambda = 0.009 \pm 0.001$ as obtained averaging the red-shift factors estimated in each single pointing (see Fig. 2).

We also searched in the range $5 - 35$ Å for the most intense lines of He-like ions of oxygen: the transitions between the $n = 2$ shell and the $n = 1$ ground state shell as the resonance line, **r** : $1s^2\ ^1S_0 - 1s2p\ ^1P_1$, the two intercombination lines (often blended), **i** : $1s^2\ ^1S_0 - 1s2p\ ^3P_{2,1}$, and the forbidden feature, **f** : $1s^2\ ^1S_0 - 1s2s\ ^3S_1$. However, because of the poor statistics of the RGS data, a blind fit procedure to the RS data around the O VII complex with a model constituted by a power law and three Gaussians (with all the parameters free, except the relative distances among the lines and the continuum power law index) did not converge. Hence, we fixed the centroid energy of the interested lines to that expected by the atomic physics after correcting for the average red-shift previously found. Interestingly, the RGS data show the existence (although with a small signal-to-noise ratio) of emission lines in the positions where the O VII complex lines are expected: this makes us confident that the line identified at $\simeq 0.19$ Å is the O VIII Ly-α transition red-shifted (on average) by $\simeq 0.009$.

A red-shift of the O VIII Ly-α line in the range $0.002 - 0.013$ (see the estimated values given in Table 3) can be explained (see also Tiengo et al. 2005) as the gravitational red-shift of the photons emitted by a plasma blob at distance R from an object with mass M, i.e. $\Delta\lambda/\lambda = 1/(g_{00})^{0.5} - 1$ with $g_{00} = 1 - 2GM/Rc^2$. As can be seen, the possibility that 4U 1700+24 hosts a white dwarf can easily be ruled out because, for the typical values of white dwarf mass and radius ($M \simeq 1$ M$_\odot$ and $R \simeq 2 \times 10^4$ km), the expected gravitational red-shift is a factor of 10 (or more) lower than the observed value. In agreement with Garcia et al. (1983), this supports the idea that 4U 1700+24 is a neutron star that accretes matter from a red giant. Assuming a neutron star mass of $\simeq 1.4$ M$_\odot$ in the 4U 1700+24 binary system, the detected red-shift range corresponds to the gravitational red-shift of a photon emitted at a distance of $160 - 1000$ km from the central object, i.e. consistent with the value found by Tiengo et al. (2005) when analyzing the 2002 *XMM*-Newton observation. Furthermore, a close inspection of Fig. 2 allows us to conclude that the red-shift of the O VII Ly-α line is variable on a time scale of few days (see the log of the observations in Table 1). In particular, the red-shifts estimated for the central observations 0151240301 and 0151240201 are $\simeq 0.004$ and $\simeq 0.012$, respectively. Since these estimates differ from the average red-shift value by more than $3 - 5\sigma$, we are confident that the effect is real. Excluding Doppler contributions due to the orbital motion of any blob of plasma around the neu-

tron star (as the associated signatures would be different to the observations presented here), we conclude that we are witnessing the re-organization of matter at a distance of a few hundred kms around the accreting object. An alternative picture would be a jet of matter (with typical velocity of $1000 - 4000$ km s^{-1}) possibly emitted away by the neutron star in an almost face-on system. The alternative condition seems to be required by the apparent lack of any periodicity and/or modulation (as we have verified via a Lomb-Scargle analysis) in the observed X-ray light curve. However, as also observed by Tiengo et al. (2005), the puzzling lack of any blue-shifted component implies the necessity of an ad-hoc geometry to explain the observations or one could invoke a uni-polar jet emitted by the neutron star.

Based on these facts, we prefer a scenario in which the mass coming from the M-type companion stellar wind (see Postnov et al. 2011 and references therein for details on the wind accretion in symbiotic X-ray binaries) is captured directly onto a small zone of the NS surface. The X-ray photons emitted are reprocessed by a blob of matter at a few hundred kms from the NS surface so that the output emission features are gravitationally red-shifted.

We estimated the 0.3-10 keV band flux to be 2.35×10^{-10} erg cm $^{-2}$ s $^{-1}$ when averaged over the four *XMM*-Newton observations. In Table 5 we also give the flux in the same band for each of the *XMM*-Newton data sets (first four rows) as well as the estimated fluxes in the energy bands $0.3 - 2$ keV and $2 - 10$ keV, respectively. As is clear, the source was in high state during the 2002 observation (see also Tiengo et al. 2005), because the flux is a factor of 2 larger than the average value, and seems to become fainter with time. This behaviour is also confirmed by the spectral analysis of seven Swift/XRT pointings towards 4U 1700+24 made in 2010 and 2012, when the source is a factor of $\simeq$ 100 fainter than in 2002. An intermediate luminosity was observed in 2005 (Masetti et al. 2006). We also observed that a black-body component is required by the best-fit model. We thus estimated the radius of the X-ray emitting region to be a few hundreds of meters, which is consistent with the expected size of a polar cap emission in a NS, and observed that this size decreases (down to a few tens of meters) as the overall X-ray luminosity decreases.

In the hypothesis that 4U1700+24 is a symbiotic X-ray binary, we expect it to behave like other candidates of this class of objects, in particular we expect the X-ray light curve to show a clear feature at the NS spin period. Typically, the observed period for a symbiotic X-ray system is in the range of minutes to hours (Lewin al. 1971, Chakrabarty & Roche 1997, Masetti et al. 2007b, Corbet et al. 2008, and Nespoli et al. 2010) but, as already stressed, the timing analysis of the 4U1700+24 light curve in the time range from 20 s to a few hours (conducted by requiring at least three full test cycles) did not show any significant feature[6]. A much more detailed analysis will be presented elsewhere.

If the source is a member of the X-ray pulsar class, the absence of a periodicity is also expected. Considering the X-ray pulsar average properties as given in Kargaltsev et al. (2012), from their relation $L_X = \eta\dot{E}$, where L_X is the $0.5 - 8$ keV luminosity and $\dot{E}$ is the spin-down energy rate (related to the NS period P and first period derivative $\dot{P}$ by $\dot{E} \simeq 10^{46}\dot{P}/P^3$ in cgs units), and assuming an average efficiency $\eta = 10^{-4}$, we obtained $\dot{E} \simeq 10^{37} - 10^{38}$ erg s^{-1}. Since the measured $\dot{P}$ values are in the range $\sim 10^{-13} - 10^{-20}$ s s^{-1} (see the on-line catalogue http : //www.astro.ufl.edu/ anuviswanathan/cgi − bin/psrcat.htm and also Becker 2001), we get P in the range $2 \times 10^{-4} - 10^{-1}$ s, which is clearly not detectable in the *XMM*-Newton and Swift data analysed in this work. Interestingly enough, assuming a polar cap model for the wind accreting NS (see e.g. Becker et al. 2012), it is possible to estimate the NS surface magnetic field which turns out to be $\lesssim 2 \times 10^{10}$ G, i.e. in agreement with the typical magnetic field values of the X-ray emitting pulsars.

Obviously, a long *XMM*-Newton observation or a planned exposure with the pn camera in timing mode could allow us to infer the NS period.

Acknowledgements. This paper is based on observations by *XMM*-Newton, an ESA science mission with instruments and contributions directly funded by ESA Member States and NASA. Part of this work is based on archival data, software or on-line services provided by the ASI Science Data Center (ASDC), Italy. AAN is grateful to Sara A. A. Nucita for the interesting discussions while preparing this manuscript. MDS thanks the Department of Mathematics and Physics *E. De Giorgi* at the University of Salento and the astrophysics group for the hospitality.

[6] The absence of a clear periodicity is not new in these kinds of objects; see e.g. the case of XTE J1743-363 described in Bozzo et al. (2013).

References

Armas-Padilla, M., et al., 2013, arxiv: 1308.4326.
Arnaud, K., Dorman, B., & Gordon, C., 2007, ApJ, *An X-ray Spectral Fitting Package - User's Guide for version 12.4.0*, Heasarc Astrophysics Science Division.
Becker, P.A., 2001, Proceedings of the conference *X-ray Astronomy '99: Stellar Endpoints, AGN & the Diffuse X-ray Background*, eds N.White et al., AIP Conference Proceedings 599, p13-24.
Becker, P.A., et al., 2012, ApJ, 544, 123.
Benlloch, S., Wilms, J., Edelson, R., Yaqoob, T, & Staubert, R., 2001, ApJ, 562, L121.
Bozzo, E., et al., 2013; A&A, 556, A30.
Burrows, D. N., et al. 2005, Space Science Review, 120, 165.
Cash, W., 1979, ApJ, 228, 939.
Chakrabarty, D., & Roche, P. 1997, ApJ, 489, 254.
Cooke, B.A., et al., 1978, MNRAS, 182, 489.
Corbet, R.H.D., Sokoloski, J.L., Mukai, K., Markwardt, C.B., & Tueller, J. 2008, ApJ, 675, 1424.
Dal Fiume, D., et al., 1990, Il Nuovo Cimento, 13C, 481.
Dere, K.P., 2001, ApJSS, 134, 331.
Dickey, J.M., & Lockman, F.J., 1990, ARA&A, 28, 215.
Edelson R. A., et al., 2002, ApJ, 568, 610.
Forman, W., et al., 1978, ApJS, 38, 357.
Galloway, D.K., Sokoloski, J.L., & Kenyon, S.J. 2002, ApJ, 580, 1065.
Garcia, M.R., et al., 1983, ApJ, 267, 291.
Gaudenzi, S., & Polcaro, V.F. 1999, A&A, 347, 473.
González-Galán, A., et al., 2012, A&A, 537, A66.
Guainazzi, M., & Bianchi, S., 2007, MNRAS, 374, 1290.
Hinkle, K.H., et al., 2006, ApJ, 641, 479.
Jansen, F., et al., 2001, A&A, 365, L1.
Kargaltsev, O., Durant, M., Pavlov, G.G., & Garmire, G., 2012, ApJ Sup. Ser., 201, 37.
Lewin, W. H. G., Ricker, G. R., & McClintock, J. E., 1971, ApJ, 169, 17.
Lü, G.-L., et al., 2012, MNRAS, 424, 2265.
Marcu, D.M., et al., 2011, ApJ, 742, L11.
Masetti, N., et al., 2002, A&A, 382, 104.
Masetti, N., Orlandini, M., Palazzi, E., Amati, L., & Frontera, F. 2006, A&A, 453, 295.
Masetti, N., et al., 2007a, A&A 464, 277.
Masetti, N., Landi, R., Pretorius, M.L., et al., 2007b, A&A, 470, 331.
Masetti, N., Nucita, A.A., & Parisi, P., 2012, A&A, 544, 114.
Mattana, F., et al., 2006, A&A, 460, L1.

Nandra, K., et al., 1997, ApJ, 476, 70.
Nespoli, E., Fabregat, J., & Mennickent, R.E., 2010, A&A, 516, A94.
Nucita, A.A., Carpano, S., & Guainazzi, M., 2007, A&A, 474, L1.
Patel, S.K., et al., 2007, ApJ, 657, 994.
Paul, B., Dotani, T., Nagase, F., Mukherjee, U., & Naik, S. 2005, ApJ, 627, 915.
Porquet, D., & Dubau, J., 2000, A&AS, 143, 495.
Postnov, K., et al., 2011, Proceedings of the 8th INTEGRAL Workshop *The Restless Gamma-ray Universe* (INTEGRAL 2010). September 27-30 2010. Dublin Castle, Dublin, Ireland. Published online at $http://pos.sissa.it/cgi-bin/reader/conf.cgi?confid=115$, id.15. See also arXiv:1110.1156.
Rea, N., et al., 2005, MNRAS, 364, 1229.
Scargle, J.,D., 1982, ApJ, 263, 835.
Strüder, L., et al., 2001, A&A, 365, L18.
Tiengo, A., et al., 2005, A&A, 441, 283.
Timmer, J., & Koenig, M., 1995, A&A, 300, 707.
Turner, M.J.L., et al., 2001, A&A, 365, L27.
Vaughan, S., Edelson, R., Warwick, R.S., & Uttly, P., 2003, MNRAS, 345, 1271.
XMM-Newton User's Handbook, 2009, Issue 2.7 (Eds. Ness J.-U et al.).
XRPS User's manual, 2008, Issue 2.6 (Eds. Ehle M. et al.).